P-Heterocyclic carbenes as effective catalysts for the activation of single and multiple bonds. A theoretical study†‡§

Markus Rullich,[a] Ralf Tonner[b] and Gernot Frenking*[b]

Received (in Montpellier, France) 19th March 2010, Accepted 24th June 2010
DOI: 10.1039/c0nj00208a

Quantum chemical calculations at the DFT (B3LYP) and *ab initio* level (CCSD(T)) have been carried out for the transition states and reaction products of the addition reactions of H_2, NH_3, CH_4, H_2O, C_6H_6, C_2H_6, C_2H_4, C_2H_2, CH_3Cl, CH_3F and SiH_4 to model *N*-heterocyclic carbenes (NHCs) and *P*-heterocyclic carbenes (PHCs). The calculations show that PHCs have substantially lower activation barriers than NHCs for breaking the single bonds H–H, O–H, N–H, C–H, C–F, C–Cl and Si–H, as well as the π-bonds in benzene, ethylene and acetylene. The main reason for the higher reactivity of PHCs is their energetically lower-lying LUMO compared to NHCs. The energy level of the LUMO and the electrophilicity of PHCs strongly depends on pyramidalization at the carbene centre. Bulky ligands stabilize intrinsically unstable PHCs because they enforce a more planar arrangement at the carbene centre, which enhances the π-donation from the phosphorus lone-pair MO to the formally empty p(π) orbital at the divalent carbon atom. This raises the energy level of the LUMO but the higher reactivity of the PHC is preserved.

1. Introduction

The introduction of *N*-heterocyclic carbenes (NHCs) as stable molecules into synthetic chemistry by Arduengo *et al.* in 1991[1] and the synthesis of the first stable carbenes by Bertrand in 1988[2] sparked enormous experimental and theoretical activities in organic and organometallic chemistry.[3] The interest in NHCs became even stronger after the finding that transition metal complexes that carry NHC ligands may serve as powerful catalysts for numerous chemical reactions.[3c] Very recently, Frey *et al.* reported in a combined theoretical/experimental study that a particular class of stable carbenes is capable of splitting H_2 and NH_3 by nucleophilic activation of H–H and N–H bonds.[4] Calculations showed that the activation barrier for the addition of H_2 and NH_3 to cyclic and acyclic (alkyl)-(amino)carbenes is clearly lower than for H_2 and NH_3 addition to NHCs.[5] Experimental studies demonstrated that diamino-carbenes do not react with H_2 at 35 °C, while (alkyl)(amino)-carbenes readily add H_2 and NH_3 (Scheme 1). The authors suggested that suitably modified carbenes might serve as "catalytic systems capable of transforming NH_3 efficiently into useful amino compounds".[4]

We became interested in the work of Bertrand and co-workers[4] in the field of carbenes due to our ongoing theoretical research in low-coordinated carbon compounds such as divalent carbon(0) species[6] ("carbones"), which exhibit unusual properties.[7] The finding that substituting one amino group in NHCs by an alkyl substituent lowers the activation barrier for the addition of H_2 and NH_3 led us to carry out a systematic theoretical investigation of the reaction course of the addition reactions of various saturated and unsaturated compounds to heterocyclic carbenes.[8] In particular, we were interested in the effect on the activation barrier of addition reactions achieved by substituting the nitrogen atom in NHCs with a phosphorus atom, thus yielding *P*-heterocyclic carbenes (PHCs). Following the synthesis of the first stable PHC by Bertrand and co-workers in 2005,[9] which is a *P*-aryl substituted derivative of **5P** (Scheme 2), several theoretical and experimental studies have been devoted to this new class of compounds.[10] Here we report on quantum chemical calculations that predict PHCs have substantially lower activation barriers than NHCs for breaking the single

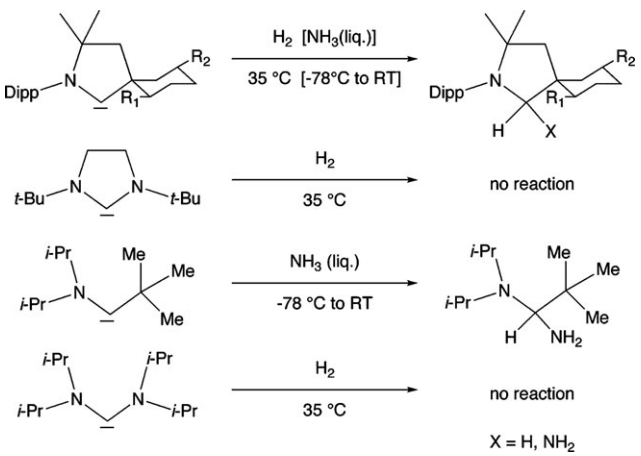

Scheme 1 Summary of the experimental results reported in ref. 4. The experimental studies were carried out for $R_1 = R_2 = H$ and for R_1 = Me, R_2 = *i*-propyl.

[a] *Bremen Center for Computational Materials Science (BCCMS), Universität Bremen, 28359 Bremen, Germany*
[b] *Fachbereich Chemie, Philipps-Universität Marburg, Hans-Meerwein-Strasse, D-35043 Marburg, Germany. E-mail: frenking@chemie.uni-marburg.de; Fax: +49 6421-282-5566*
† Dedicated to Wolfgang Kirmse, a pioneer of carbene chemistry, on the occasion of his 80th birthday.
‡ This article is part of a themed issue on Main Group chemistry.
§ Electronic supplementary information (ESI) available: Table S1. Coordinates and energies of the calculated molecules at B3LYP/def-TZVP. See DOI: 10.1039/c0nj00208a

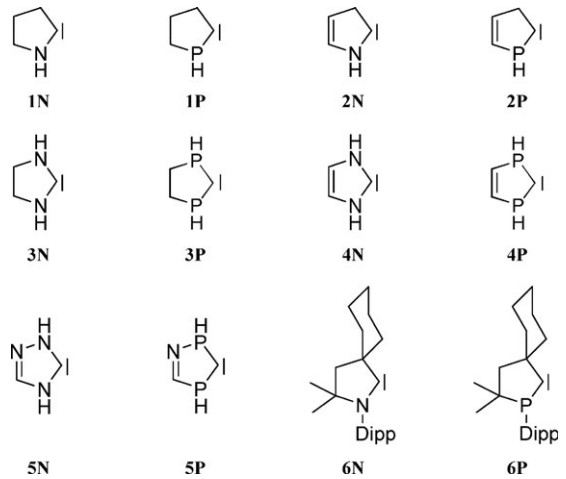

Scheme 2 An overview of the heterocyclic carbenes that have been calculated in this work.

bonds H–H, O–H, N–H, C–H, C–C, C–F, C–Cl and Si–H in H_2, NH_3, CH_4, H_2O, C_6H_6, C_2H_6, C_2H_4, C_2H_2, CH_3Cl, CH_3F and SiH_4, as well as the π-bonds in benzene, ethylene and acetylene.

2. Theoretical details

The geometry optimizations were carried out at the B3LYP/def-TZVP level of theory[11] using the program package Gaussian03.[12] The Hessian matrices were calculated at the same level of theory in order to verify that the optimized structures were minima or transition states on the potential energy surface. Additional single-point energy calculations were performed at CCSD(T)/cc-pVTZ[13] using the B3LYP/def-TZVP-optimized structures. The latter calculations were carried out using the program MOLPRO.[14] Unless otherwise noted, the energies discussed in this paper were obtained at the CCSD(T)/cc-pVTZ//B3LYP/def-TZVP level of theory. We decided to use the relative energies, which are not augmented by ZPE or thermal correction terms, because we were searching for electronic factors that influence the barriers and reaction energies. The S/T gaps were calculated as the difference between singlet and triplet ground state energies.

3. Results

Scheme 2 shows the NHCs and PHCs that were studied in our work. Two series of reactions have been investigated. We first optimized the transition states and reaction products for the addition of H_2, H_2O, NH_3, CH_4, C_6H_6, C_2H_6, C_2H_4, C_2H_2, CH_3F, CH_3Cl and SiH_4 to the parent NHC **1N** and PHC **1P**. The results of this part will be presented first. In a second step, we optimized the transition states and reaction products for the addition of H_2 to NHCs **1N–6N** and PHCs **1P–6P**. The latter results are discussed further below. The calculations showed that the reactants for the addition reactions yield weakly-bonded precursor complexes that are not relevant for the present work; therefore, they are not reported here. For some reactions where the activation barriers are very small, we found that the transition state is energetically lower-lying than the separated reactants. The activation barriers may, in such cases, even become negative with respect to the reactants. If there is a possibility of the generation of diastereomers, the pathway with the lowest barrier is presented.

3.1 Addition of H_2 to 1N and 1P

Fig. 1 shows the optimized reactants, transition states and products along the reaction course for the addition of H_2 to parent NHC **1N** and PHC **1P**. The strongly exothermic addition of H_2 to **1N** ($\Delta E_R = -57.1$ kcal mol^{-1}) proceeds with a moderate barrier of 23.6 kcal mol^{-1}. While this barrier is very similar to the previously calculated value by Frey *et al.*[4] (23.7 kcal mol^{-1}), we find a stronger exothermic reaction (compared to −45.3 kcal mol^{-14}). A much lower barrier of only 3.8 kcal mol^{-1} is predicted for H_2 addition to **1P**. The latter reaction is even more exothermic ($\Delta E_R = -100.9$ kcal mol^{-1}) than the former. The H–H distance in the transition state for H_2 addition to **1P** (0.810 Å) is only slightly stretched in comparison to the calculated equilibrium distance (0.744 Å), while the transition state for the hydrogenation of **1N** has a much longer H–H distance (1.113 Å). The structure of the transition state is thus in agreement with the Hammond postulate.[15] The geometries of the transition states show that the formation of C–H bonds to the carbene carbon atoms takes place in a concerted but highly asymmetric way, where one C–H bond is formed much earlier than the other.

3.2 Addition of H_2O, NH_3, CH_4 and SiH_4 to 1N and 1P

Fig. 2 shows the optimized reactants, transition states and products along the reaction course for the addition of H_2O,

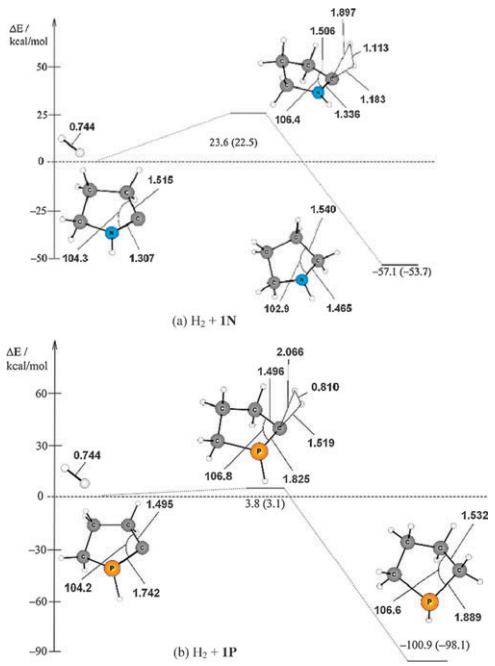

Fig. 1 Calculated reaction profiles showing the reactants, transition states and products for the reactions of (a) H_2 + **1N** and (b) H_2+**1P**. Energy values (in kcal mol^{-1}) at CCSD(T)/cc-pVTZ//B3LYP/def-TZVP, the values at B3LYP/def-TZVP are given in parentheses. Distances are given in Å and angles in degrees.

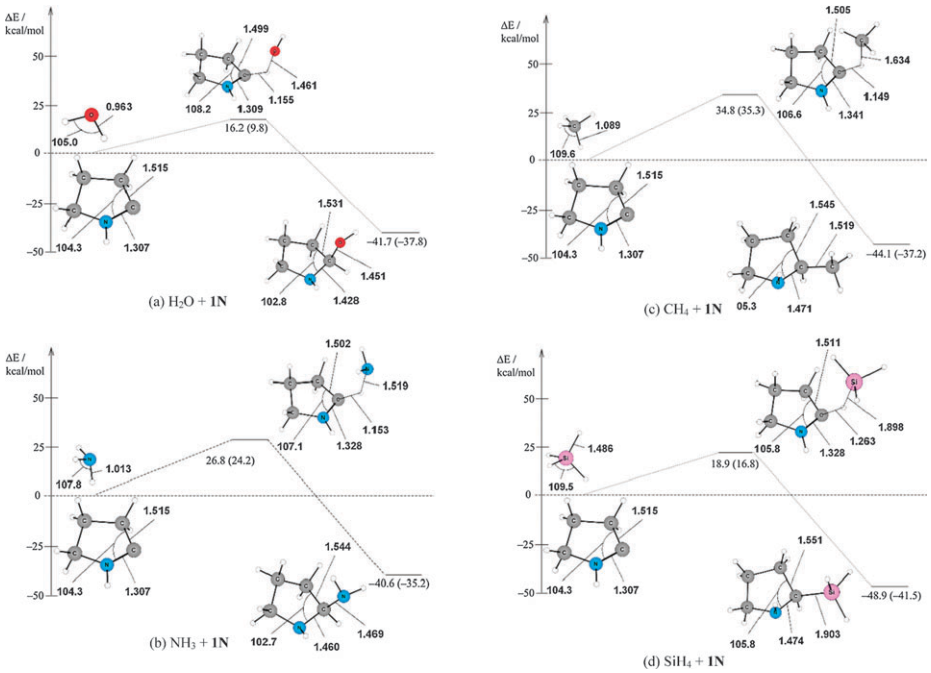

Fig. 2 Calculated reaction profiles showing the reactants, transition states and products for the reactions of (a) H_2O + **1N**, (b) NH_3 + **1N**, (c) CH_4 + **1N** and (d) SiH_4 + **1N**. Energy values (in kcal mol^{-1}) at CCSD(T)/cc-pVTZ//B3LYP/def-TZVP, the values at B3LYP/def-TZVP are given in parentheses. Distances are given in Å and angles in degrees.

NH_3, CH_4 and SiH_4 to **1N**. The calculated results for the addition of H_2O, NH_3, CH_4 and SiH_4 to **1P** are shown in Fig. 3.

The calculated transition states for the addition of H_2O, NH_3, CH_4 and SiH_4 to **1N** and **1P** show that the reaction always takes place *via* initial addition of the E–H bond to the formally vacant p(π) orbital of the carbene centre. C–H bond formation in all the reactions clearly precedes the development of the C–E (E = O, N, C, Si) bond. The $C_{carbene}$–H distances in the transition states for the addition of H_2O, NH_3, and CH_4 to **1N** have a rather narrow range between 1.149–1.155 Å, while the $C_{carbene}$–H distance in the transition state for the addition of SiH_4 to **1N** is clearly longer (1.263 Å). The $C_{carbene}$–H distances in the latter transition states do not

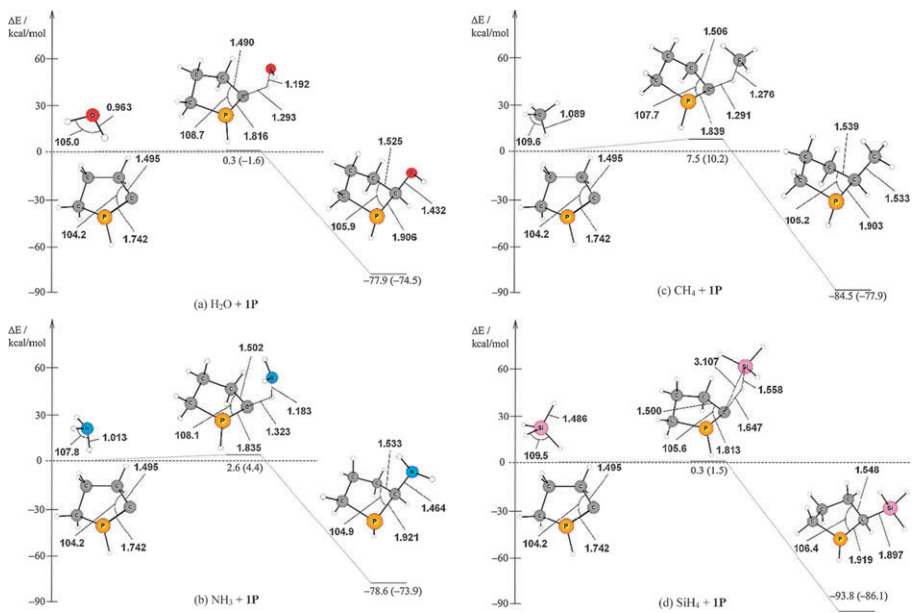

Fig. 3 Calculated reaction profiles showing the reactants, transition states and products for the reactions of (a) H_2O + **1P**, (b) NH_3 + **1P**, (c) CH_4 + **1P** and (d) SiH_4 + **1P**. Energy values (in kcal mol^{-1}) at CCSD(T)/cc-pVTZ//B3LYP/def-TZVP, the values at B3LYP/def-TZVP are given in parentheses. Distances are given in Å and angles in degrees.

correlate with the activation barriers, which are similarly high for the addition of SiH_4 (18.9 kcal mol^{-1}) and H_2O (16.2 kcal mol^{-1}), while they are clearly higher for NH_3 (26.8 kcal mol^{-1}) and particularly for CH_4 (34.8 kcal mol^{-1}).

The activation energies for the addition of H_2O, NH_3, CH_4 and SiH_4 to **1P** are significantly lower, and the reactions are much more exothermic than for the addition to **1N**. Fig. 3 shows that the barriers are only between 0.3 kcal mol^{-1} (SiH_4 and H_2O) and 7.5 kcal mol^{-1} (CH_4). The order of the activation barriers, $CH_4 > NH_3 > H_2O \approx SiH_4$, is thus the same for **1N** and **1P**. The $C_{carbene}$–H distance in the transition state for the addition of SiH_4 to **1P** is again clearly longer (1.647 Å) than in the other three transition states, where the $C_{carbene}$–H distances vary from 1.291 (CH_4) to 1.323 (NH_3) Å.

3.3 Addition of C_2H_6, CH_3F and CH_3Cl to 1N and 1P

There are two different bonds in C_2H_6, CH_3F and CH_3Cl that may coordinate to the carbene carbon atom in **1N** and **1P**, the C–H bond or the C–X (X = CH_3, F, Cl) bond. We thus calculated the reaction profiles for both sets of reactions. Fig. 4 shows the calculated transition states for the addition of the C–H bonds of the three reactants to **1N**, while Fig. 5 displays the reaction profiles for their addition to **1P**.

The transition states for the C–H addition of C_2H_6, CH_3F and CH_3Cl to **1N** and **1P** resemble the transition state for C–H addition of CH_4 (Fig. 2 and Fig. 3), where one hydrogen of the CH_3 moiety is replaced by the substituent CH_3, F and Cl, respectively. The activation barriers for the C–H addition of C_2H_6, CH_3F and CH_3Cl are, for both heterocarbenes, slightly lower than for the addition of CH_4, and the $C_{carbene}$–H distance in the transition state of the substituted species is slightly longer than in the transition state for CH_4 addition. The fluorine and chlorine atoms are tilted away from the nitrogen or phosphorus atom in the transition states for the addition of CH_3F and CH_3Cl to **1N** and **1P**, while the methyl group in the transition states for the addition of C_2H_6 is pointing towards N or P. The C–H addition reactions of C_2H_6, CH_3F and CH_3Cl to **1N** and **1P** are also slightly more exothermic than the addition of CH_4 to the heterocarbenes.

The reaction profiles for the C–X addition of C_2H_6, CH_3F and CH_3Cl to **1N** and **1P** are shown in Fig. 6 and Fig. 7, respectively. A comparison of the transition states for C–X addition with the transition states for C–H addition (Fig. 4 and Fig. 5) shows a striking difference between the two reactions. The C–X bond approaches the carbene carbon atom in **1N** and **1P** with a side-on trajectory, while the C–H addition takes place head-on with the hydrogen atom as the arrowhead. The activation barriers for the C–X addition of C_2H_6, CH_3F and CH_3Cl to **1N** are clearly higher than the barriers for C–H activation. In particular, the transition state for the C–C addition of C_2H_6 to **1N** is much higher (86.3 kcal mol^{-1}) than the C–H addition (31.0 kcal mol^{-1}). In spite of the prohibitively large activation barriers for the reactions to take place under thermal conditions, the C–X addition of C_2H_6, CH_3F and CH_3Cl to **1N** is thermodynamically favoured over the C–H addition. The data in Fig. 6 predict that the C–X addition reactions are more exothermic than the C–H addition reactions shown in Fig. 4.

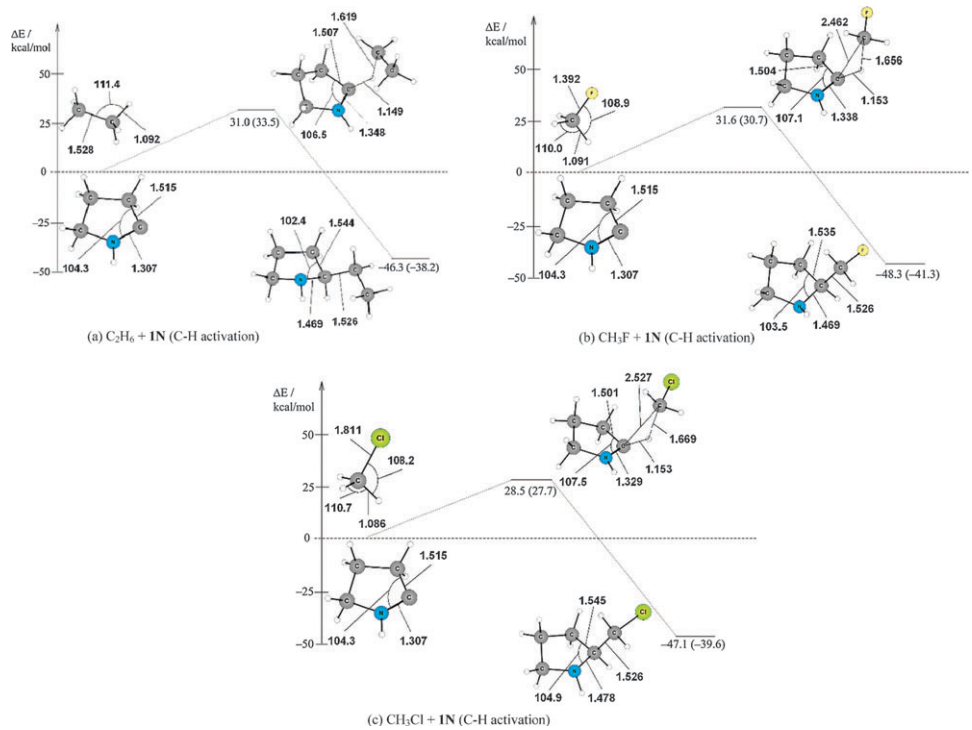

Fig. 4 Calculated reaction profiles showing the reactants, transition states and products for the C–H activation reactions of (a) C_2H_6 + **1N**, (b) CH_3F + **1N** and (c) CH_3Cl + **1N**. Energy values (in kcal mol^{-1}) at CCSD(T)/cc-pVTZ//B3LYP/def-TZVP, the values at B3LYP/def-TZVP are given in parentheses. Distances are given in Å and angles in degrees.

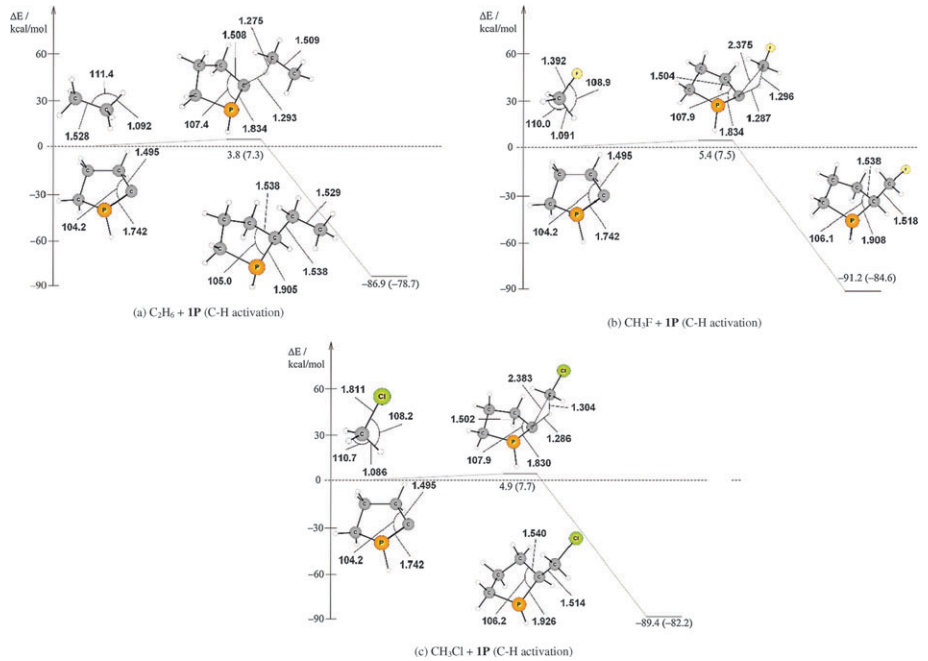

Fig. 5 Calculated reaction profiles showing the reactants, transition states and products for the C–H activation reactions of (a) C_2H_6 + **1P**, (b) CH_3F + **1P** and (c) CH_3Cl + **1P**. Energy values (in kcal mol^{-1}) at CCSD(T)/cc-pVTZ//B3LYP/def-TZVP, the values at B3LYP/def-TZVP are given in parentheses. Distances are given in Å and angles in degrees.

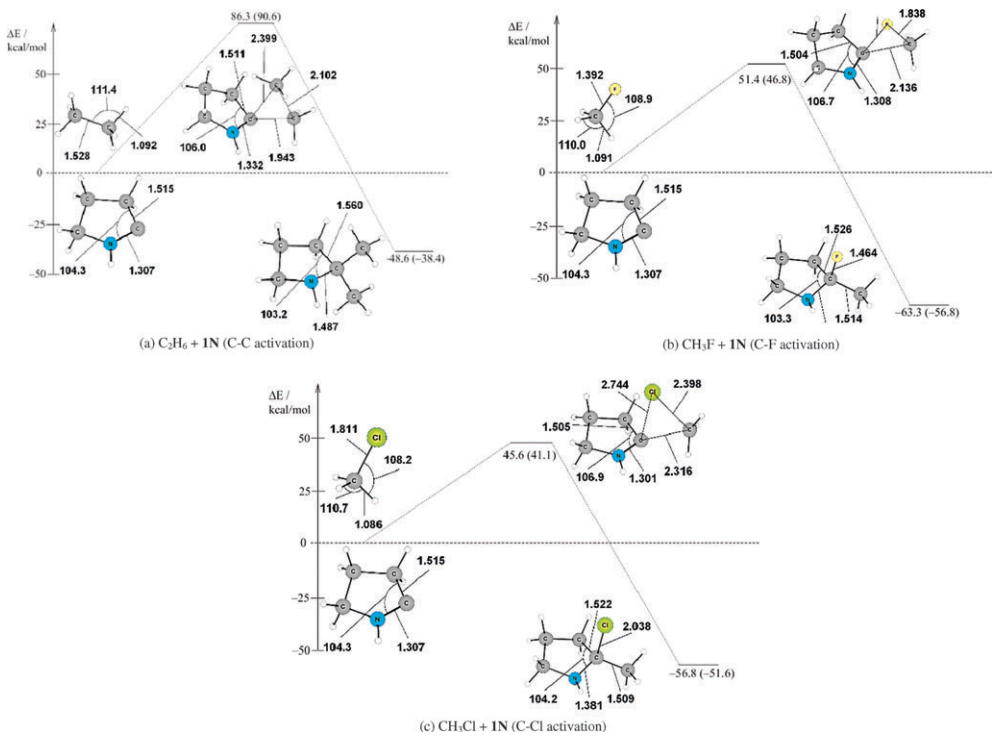

Fig. 6 Calculated reaction profiles showing the reactants, transition states and products for the C–X activation reactions of (a) C_2H_6 + **1N**, (b) CH_3F + **1N** and (c) CH_3Cl + **1N**. Energy values (in kcal mol^{-1}) at CCSD(T)/cc-pVTZ//B3LYP/def-TZVP, the values at B3LYP/def-TZVP are given in parentheses. Distances are given in Å and angles in degrees.

The reaction profiles for the C–X addition of C_2H_6, CH_3F and CH_3Cl to **1P** (Fig. 7) also show that the barriers are dramatically higher than those of the C–H addition reactions (Fig. 5). Although the latter reactions are kinetically much more favoured than the former processes, they are thermodynamically slightly disfavoured. The addition of

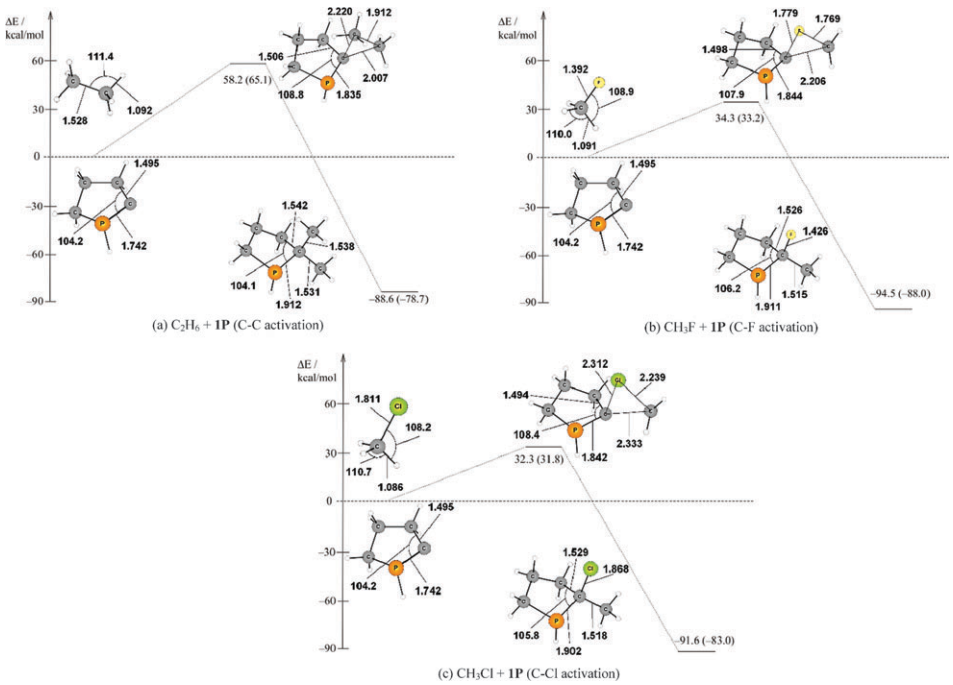

Fig. 7 Calculated reaction profiles showing the reactants, transition states and products for the C–X activation reactions of (a) C_2H_6 + **1P**, (b) CH_3F + **1P** and (c) CH_3Cl + **1P**. Energy values (in kcal mol^{-1}) at CCSD(T)/cc-pVTZ//B3LYP/def-TZVP, the values at B3LYP/def-TZVP are given in parentheses. Distances are given in Å and angles in degrees.

the C–X bonds is slightly more exothermic than the addition of the C–H bonds. For both types of addition reaction, it holds that PHC **1P** requires lower activation barriers than NHC **1N**.

3.4 Addition of C_6H_6, C_2H_4 and C_2H_2 to 1N and 1P

The addition of the unsaturated compounds C_2H_4, C_2H_2 and C_6H_6 to **1N** and **1P** may also take place in two different ways. The reactants could either add to the carbenes through

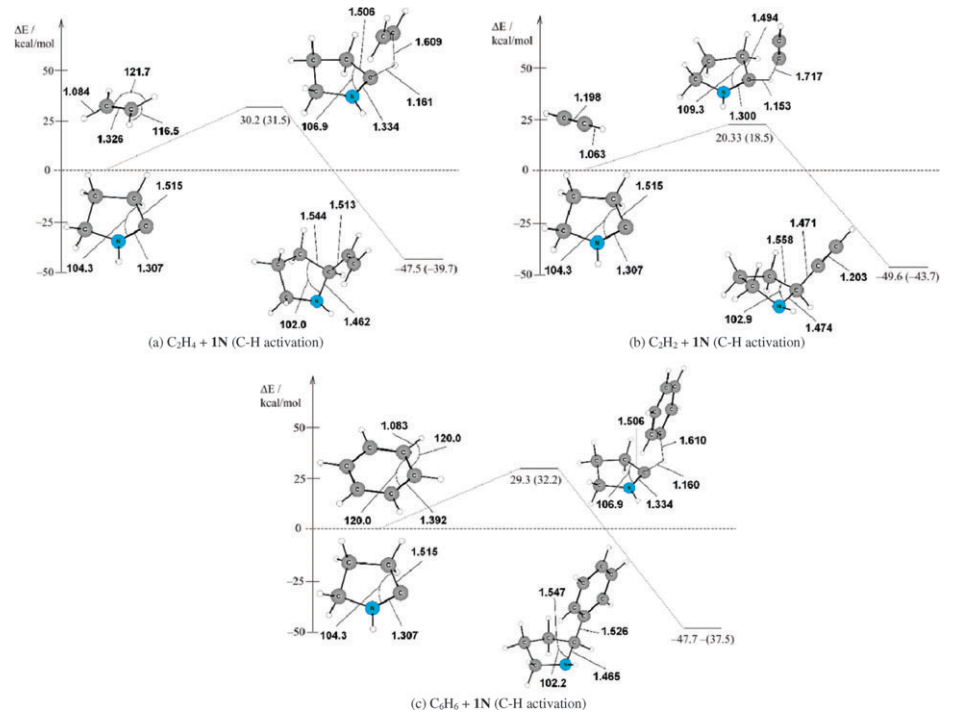

Fig. 8 Calculated reaction profiles showing the reactants, transition states and products for the C–H activation reactions of (a) C_2H_4 + **1N**, (b) C_2H_2 + **1N** and (c) C_6H_6 + **1N**. Energy values (in kcal mol^{-1}) at CCSD(T)/cc-pVTZ//B3LYP/def-TZVP, the values at B3LYP/def-TZVP are given in parentheses. Distances are given in Å and angles in degrees.

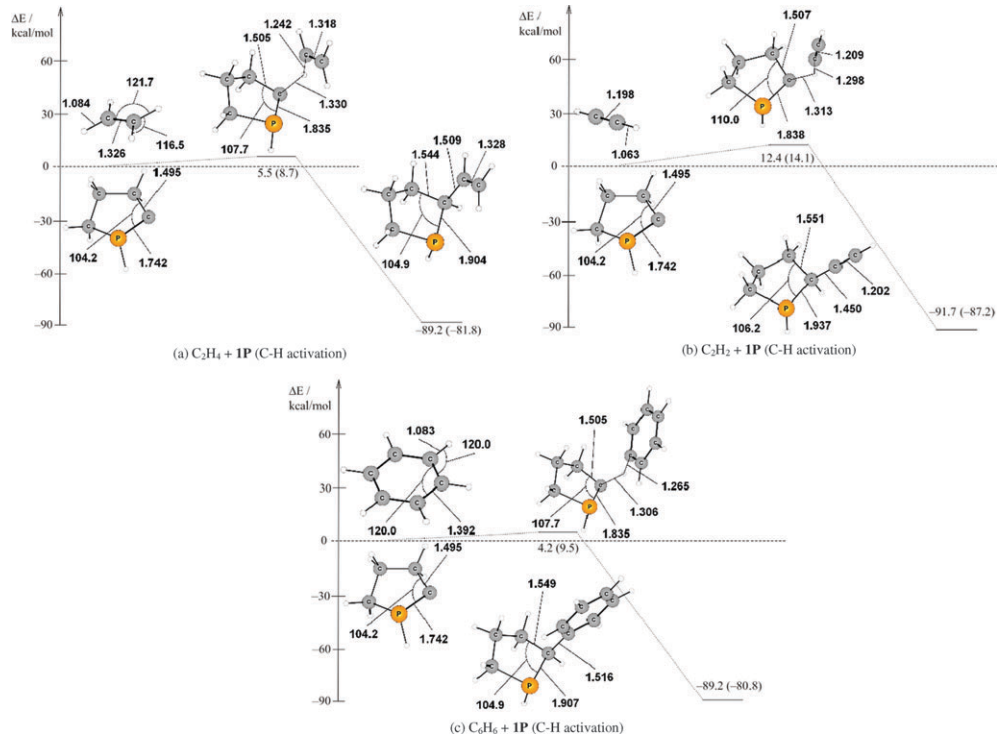

Fig. 9 Calculated reaction profiles showing the reactants, transition states and products for the C–H activation reactions of (a) C_2H_4 + **1P**, (b) C_2H_2 + **1P** and (c) C_6H_6 + **1P**. Energy values (in kcal mol^{-1}) at CCSD(T)/cc-pVTZ//B3LYP/def-TZVP, the values at B3LYP/def-TZVP are given in parentheses. Distances are given in Å and angles in degrees.

the C–H σ-bonds or they could add through the C–C π-bonds. We thus calculated the reaction profiles for both sets of reactions. Fig. 8 shows the calculated transition states for the addition of the C–H bonds of the three reactants to **1N**, while Fig. 9 presents the reaction profiles for the addition to **1P**.

The calculated transition states reveal a head-on approach of the C–H bonds to the heterocyclic carbenes. Fig. 8 shows rather late transition states, where the C–H bond being formed has rather short distances, between 1.153–1.161 Å. The activation barriers of the exothermic reactions follow the order $C_2H_4 \approx C_6H_6 > C_2H_2$. Much lower activation barriers, between 4.2–12.4 kcal mol^{-1}, are predicted for the addition of the three hydrocarbons to **1P** (Fig. 9). It is relevant to note that the addition of acetylene to **1P** has a clearly higher barrier than the addition of benzene and ethylene, which is opposite to the addition reactions to **1N**, where acetylene has the lowest activation barrier.[16] The reaction energies for the addition of C_2H_4, C_2H_2 and C_6H_6 to **1P** exhibit rather uniform values between 89.2–91.7 kcal mol^{-1}, thus being around 40 kcal mol^{-1} more favourable than the addition reactions to **1N**.

Heterocarbenes **1N** and **1P** may also add to the C–C π-bonds of the unsaturated hydrocarbons, yielding spiro compounds as reaction products. Fig. 10 and Fig. 11 show that the addition of **1N** and **1P** to the C–C π-bonds is kinetically favoured over the addition to the C–H bonds (Fig. 8 and Fig. 9). The activation barriers for the former reactions, which proceed in a side-ways approach of the respective C–C bond to **1N**, are much lower (10.6–14.9 kcal mol^{-1}) than the barriers for the latter processes (Fig. 10). The addition of C_2H_2 to **1N**, yielding the spiro product, takes place as a stepwise reaction with low activation barriers, while the other reactions are one-step processes. Note that the reaction energies become significantly less exothermic for the reaction of C_2H_4 (−41.3 kcal mol^{-1}) to C_2H_2 (−32.7 kcal mol^{-1}) and C_6H_6 (−13.9 kcal mol^{-1}). This can be explained by the weakening of the remaining π-bond in acetylene and particularly the loss of aromatic stabilization in C_6H_6.

Fig. 11 shows that the exothermic reaction energies for the addition of the π-bond of C_6H_6, C_2H_4 and C_2H_2 to **1P** has the same order as the addition to **1N**, $C_2H_4 > C_2H_2 > C_6H_6$. The calculated activation barriers suggest that the reactions take place with essentially no barrier. It is interesting to note that the addition of C_2H_2 to **1P**, yielding the spiro compound as the product, takes place in one step, while the addition of C_2H_2 to **1N** proceeds *via* a multi-step pathway (Fig. 10).

3.5 Addition of H_2 to 1N–6N and 1P–6P

The previous results show that the addition of C–X single bonds and C–C π-bonds to model PHC **1P** always has a lower activation barrier than the addition to model NHC **1N**. We also calculated reaction profiles for the addition of H_2 to different NHCs, **1N–6N**, and to their analogous PHCs, **1P–6P** (Scheme 2). Fig. 12 shows the theoretically predicted reaction profiles and transition states, as well as the reactants and products for the addition reactions to **2N–6N**. The reaction profile for the hydrogenation of **1N** has already been shown in Fig. 1a.

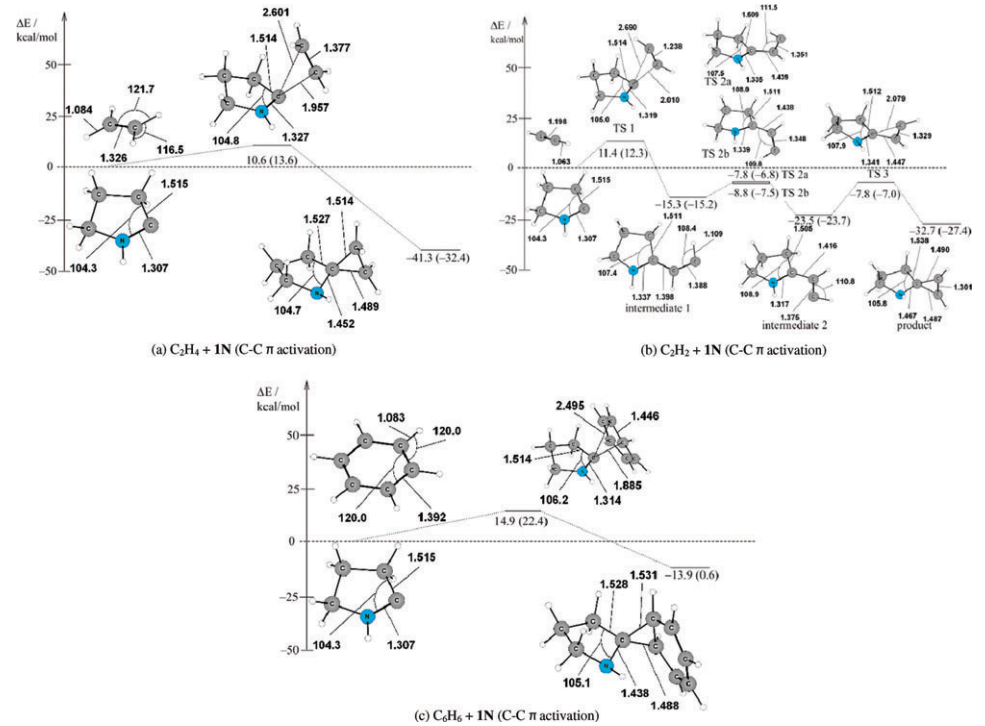

Fig. 10 Calculated reaction profiles showing the reactants, transition states and products for the C–C π-activation reactions of (a) C_2H_4 + **1N**, (b) C_2H_2 + **1N** and (c) C_6H_6 + **1N**. Energy values (in kcal mol^{-1}) at CCSD(T)/cc-pVTZ//B3LYP/def-TZVP, the values at B3LYP/def-TZVP are given in parentheses. Distances are given in Å and angles in degrees.

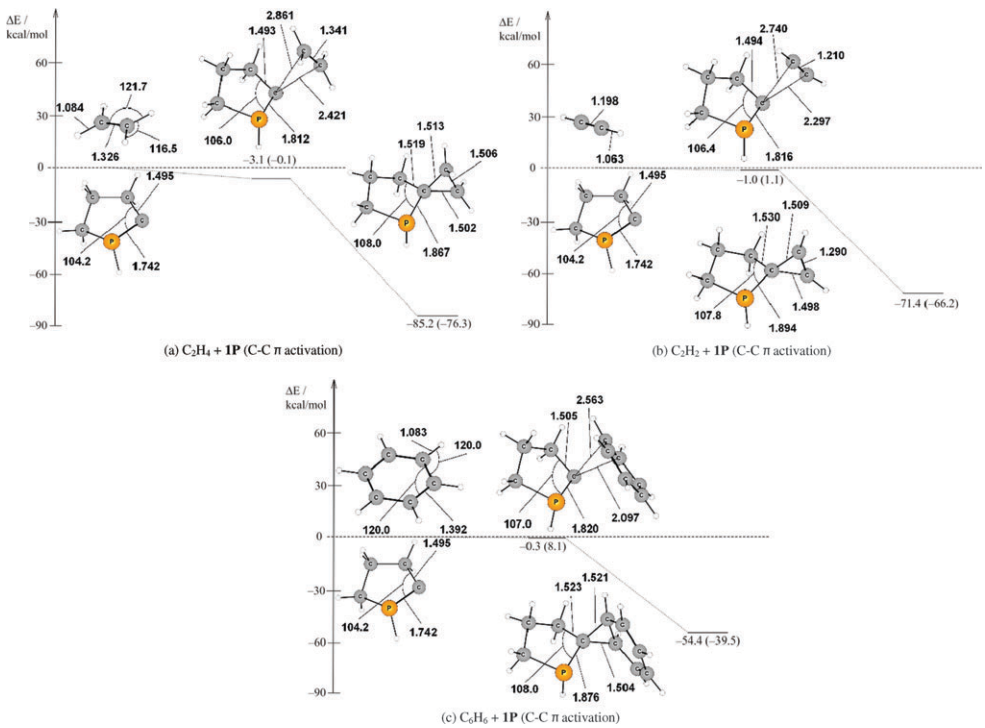

Fig. 11 Calculated reaction profiles showing the reactants, transition states and products for the C–C π-activation reactions of (a) C_2H_4 + **1P**, (b) C_2H_2 + **1P** and (c) C_6H_6 + **1P**. Energy values (in kcal mol^{-1}) at CCSD(T)/cc-pVTZ//B3LYP/def-TZVP, the values at B3LYP/def-TZVP are given in parentheses. Distances are given in Å and angles in degrees.

Unsaturated NHC **2N** has a slightly higher barrier for the hydrogenation reaction than saturated NHC **1N**, but the former process is slightly more exothermic than the latter. The introduction of a second nitrogen atom into the α-position significantly raises the activation barrier for saturated NHC **3N** and particularly for unsaturated NHC **4N**,

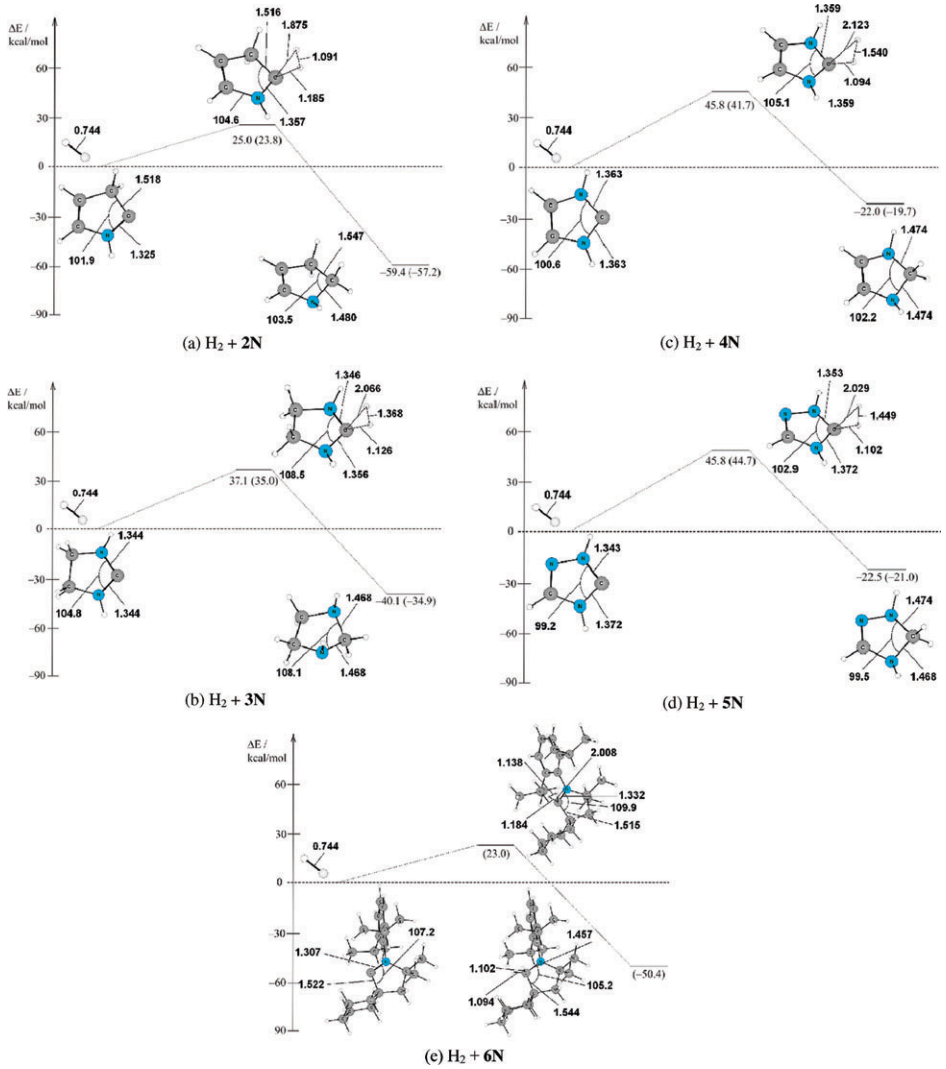

Fig. 12 Calculated reaction profiles showing the reactants, transition states and products for the reactions of (a) H_2 + **2N**, (b) H_2 + **3N**, (c) H_2 + **4N**, (d) H_2 + **5N** and (e) H_2 + **6N**.[17] Energy values (in kcal mol^{-1}) at CCSD(T)/cc-pVTZ//B3LYP/def-TZVP, the values at B3LYP/def-TZVP are given in parentheses. Distances are given in Å and angles in degrees.

where the barrier becomes 45.8 kcal mol^{-1} (Fig. 11c). The introduction of a further nitrogen atom into the β-position of unsaturated NHC **5N** has no effect on the barrier height. Note that the calculated activation energy (23.0 kcal mol^{-1} at B3LYP/def-TZVP)[17] and the reaction energy (−50.4 kcal mol^{-1}) for the hydrogenation of real NHC **6N**, employed by Frey *et al.*[4] in their experimental work, are nearly the same as for model NHC **1N** (Fig. 1a). All the hydrogenation reactions of **1N–6N** are strongly exothermic.

Fig. 13 shows the calculated data for the hydrogenation reactions of PHCs **2P–6P**. The theoretically predicted activation barriers are always lower and the reactions are much more exothermic compared with the hydrogenation of NHCs **2N–6N** (Fig. 12). The trend for the activation barriers of the PHCs runs parallel to the trend of the NHCs, except for **6P**. The activation energy for the hydrogenation of saturated real system **6P** (17.7 kcal mol^{-1}, B3LYP/TZVP[17]) is clearly higher than for saturated model compound **1P** (3.1 kcal mol^{-1}), while the barriers for their respective NHCs are nearly the same. The reason for this finding, and for the other results, is discussed in the following section.

4. Discussion

The calculated reaction profiles for the addition of various substrates to NHCs and PHCs poses questions about the trends predicted by the energies calculated, and particularly by the calculated activation barriers. Fig. 14 displays the calculated activation energies with increasing barrier height for the addition reactions of the investigated substrates to NHC **1N**. The calculated activation barriers for the addition reactions to **1P** are also shown. Clearly the addition reactions with **1P** always possess lower activation energies than the addition reactions with **1N**. Nearly all the addition reactions with PHC **1P** are predicted to exhibit very low barriers (< 10 kcal mol^{-1}), except for the reactions of the C–H single bond of acetylene, the C–F and C–Cl bonds of the halomethanes CH_3F and CH_3Cl, and the C–C single bond of ethane. We

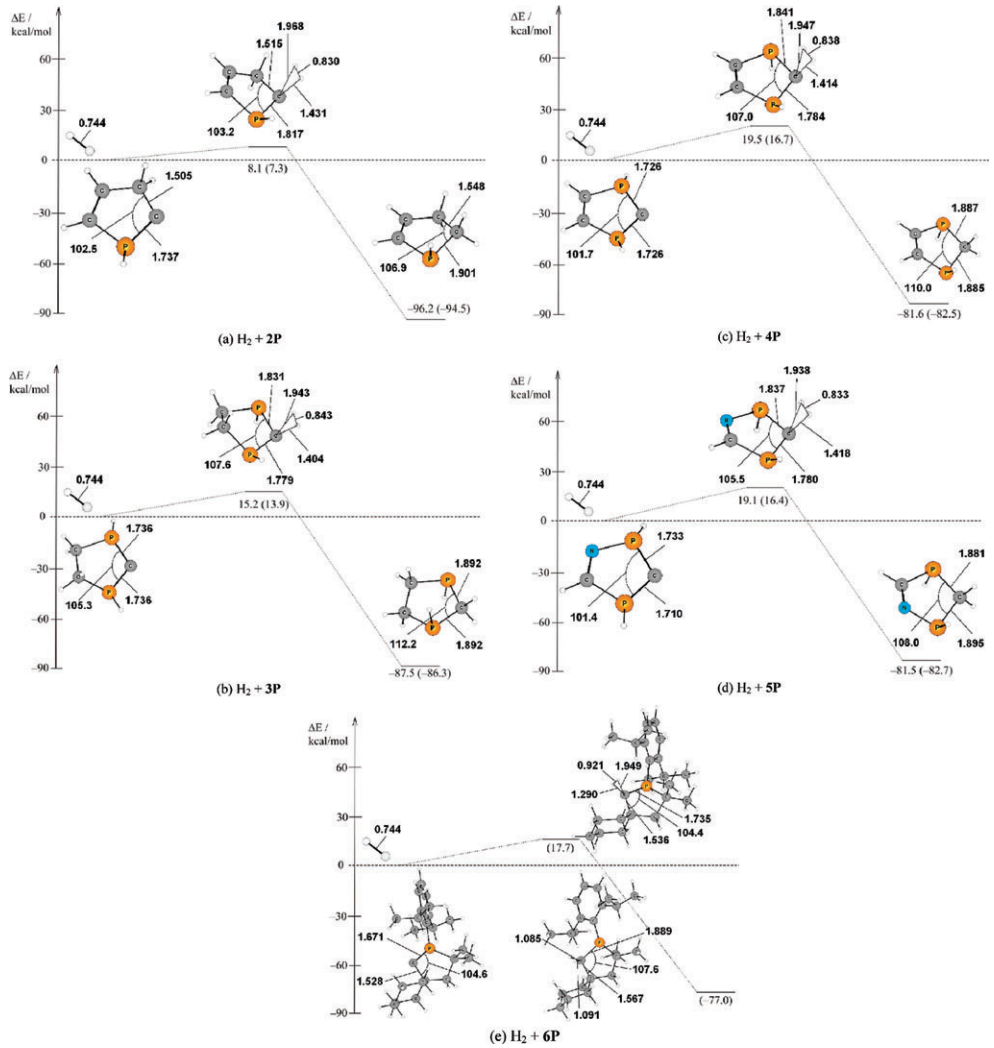

Fig. 13 Calculated reaction profiles showing the reactants, transition states and products for the reactions of (a) H_2 + **2P**, (b) H_2+**3P**, (c) H_2+**4P**, (d) H_2+**5P** and (e) H_2+**6P**.[17] Energy values (in kcal mol^{-1}) at CCSD(T)/cc-pVTZ//B3LYP/def-TZVP, the values at B3LYP/def-TZVP are given in parentheses. Distances are given in Å and angles in degrees.

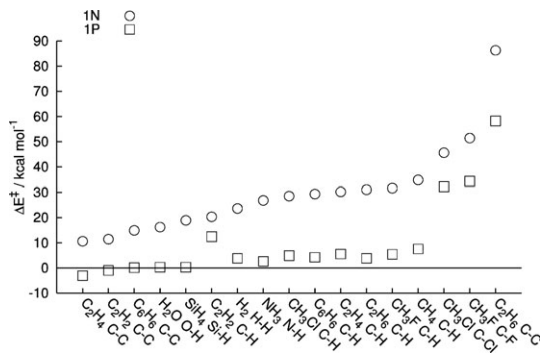

Fig. 14 A plot of the calculated activation barriers, $\Delta E^{\ddagger}$, with increasing barrier height for the addition reactions of the investigated substrates to NHC **1N** (top) and PHC **1P** (bottom). Energy values (in kcal mol^{-1}) at CCSD(T)/cc-pVTZ//B3LYP/def-TZVP.

used the electronic energies $\Delta E^{\ddagger}$ without ZPE corrections because we are interested in the electronic reasons for the trends in the activation barriers. Table 1 gives activation barriers and reaction energies, which include ZPE contributions. The data show that the ZPE corrections do not change the trends and that the absolute values change only by up to ~2 kcal mol^{-1}. We also wish to point out that the *ab initio* calculations at the CCSD(T)/cc-pVTZ level give very similar results for $\Delta E^{\ddagger}$ and ΔE_R compared to the B3LYP/def-TZVP calculations, and that the trends given at the two levels of theory are qualitatively the same.

The search for an explanation of the trends in the activation energies of the different substrates in the addition reactions proved difficult. Neither the frontier orbitals nor the atomic charge distribution provide a simple explanation. The HOMO of the substrates is not a useful indicator for the reaction because the highest lying MO is, in some cases, a lone pair orbital that is not directly involved in the addition reactions, while, in other cases, it is highly delocalized. An explanation for the trends could perhaps be given by an energy decomposition analysis (EDA) of the transition states. We did not carry out such an extensive study because we are mainly interested in the difference in reactivity between NHCs and PHCs rather

Table 1 Calculated activation energies, $\Delta E^{\ddagger}$, and reaction energies, ΔE_R, at CCSD(T)/cc-pVTZ//B3LYP/def-TZVP and (in parentheses) at B3LYP/def-TZVP for the reaction of **1N** and **1P** with diverse substrates. Zero point energy-corrected values are given in italics. Energy values are given in kcal mol^{-1}

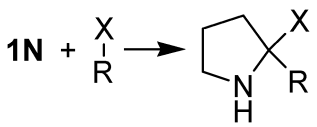

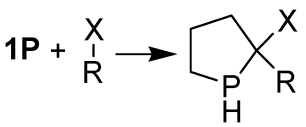

R–X	E^a	X	$\Delta E^{\ddagger}$	ΔE_R	$\Delta E^{\ddagger}$	ΔE_R
H_2	H	H	23.6 (22.5)	−57.1 (−53.7)	3.8 (3.1)	−100.9 (−98.1)
			25.8 (*24.8*)	*−48.2* (*−44.8*)	*6.6* (*5.9*)	*−90.7* (*−87.9*)
NH_3	N	H	26.8 (24.2)	−40.6 (−35.2)	2.6 (4.4)	−78.6 (−73.9)
			25.9 (*23.4*)	*−36.3* (*−30.8*)	*2.7* (*4.5*)	*−72.8* (*−68.1*)
CH_4	C	H	34.8 (35.3)	−44.1 (−37.2)	7.5 (10.2)	−84.5 (−77.9)
			33.9 (*34.5*)	*−39.3* (*−32.4*)	*7.9* (*10.6*)	*−78.5*(*−71.9*)
H_2O	O	H	16.2 (9.8)	−41.7 (−37.7)	0.3 (−1.6)	−77.9 (−74.5)
			16.6 (*10.2*)	*−37.1* (*−33.2*)	*0.7* (*−1.2*)	*−71.8* (*−68.5*)
C_6H_6	C	H	29.3 (32.2)	−47.7 (−37.5)	4.2 (9.5)	−89.2 (−80.8)
			28.0 (*30.9*)	*−44.7* (*−34.6*)	*3.5* (*8.9*)	*−84.9* (*−76.4*)
	C	C	14.9 (22.4)	−13.9 (0.6)	−0.3 (8.1)	−54.4 (−39.5)
			15.8 (*23.3*)	*−11.5* (*3.0*)	*1.1* (*9.5*)	*−50.6* (*−35.6*)
C_2H_6	C	H	31.0 (33.5)	−46.3 (−38.2)	3.8 (7.3)	−86.9 (−78.7)
			29.6 (*32.2*)	*−42.5* (*−34.3*)	*3.5* (*7.1*)	*−81.6* (*−73.4*)
	C	C	86.3 (90.6)	−48.6 (−38.4)	58.2 (65.1)	−88.6 (−78.7)
			85.5 (*89.8*)	*−45.4* (*−35.2*)	*59.4* (*66.2*)	*−83.9* (*−74.0*)
C_2H_4	C	H	30.2 (31.5)	−47.5 (−39.7)	5.5 (8.7)	−89.2 (−81.8)
			19.2 (*30.4*)	*−43.7* (*−35.9*)	*5.3* (*8.5*)	*−83.9* (*−76.5*)
	C	C	10.6 (13.6)	−41.3 (−32.4)	−3.1 (−0.1)	−85.2 (−76.3)
			21.1 (*15.0*)	*−37.2* (*−28.3*)	*−1.6* (*1.5*)	*−79.5* (*−70.6*)
C_2H_2	C	H	20.3 (18.5)	−49.6 (−43.7)	12.4 (14.1)	−91.7 (−87.2)
			21.3 (*19.5*)	*−44.5* (*−38.6*)	*12.7* (*14.4*)	*−85.3* (*−80.8*)
	C	C	11.4 (12.7)	−32.7 (−27.4)	−1.0 (1.1)	−71.4 (−66.2)
			13.4 (*14.8*)	*−28.3* (*−23.0*)	*1.1* (*3.3*)	*−65.5* (*−60.4*)
CH_3Cl	C	H	28.5 (27.7)	−47.1 (−39.6)	4.9 (7.7)	−89.4 (−82.2)
			27.3 (*26.5*)	*−43.4* (*−35.8*)	*4.3* (*7.0*)	*−84.1* (*−76.9*)
	C	Cl	45.6 (41.1)	−56.8 (−51.6)	32.3 (31.8)	−91.6 (−83.0)
			45.9 (*41.5*)	*−53.6* (*−48.5*)	*33.1* (*32.6*)	*−87.1* (*−78.5*)
CH_3F	C	H	31.6 (30.6)	−48.3 (−41.3)	5.4 (7.5)	−91.2 (−84.6)
			30.4 (*29.4*)	*−44.6* (*−37.6*)	*5.1* (*7.3*)	*−85.8* (*−79.2*)
	C	F	51.4 (46.8)	−63.3 (−56.8)	34.3 (33.2)	−94.5 (−88.0)
			51.5 (*46.9*)	*−60.3* (*−53.8*)	*35.1* (*34.0*)	*−90.2* (*−83.7*)
SiH_4	Si	H	18.9 (16.8)	−48.9 (−41.5)	0.3 (1.5)	−93.8 (−86.1)
			19.8 (*19.0*)	*−44.1* (*−36.7*)	*0.9* (*2.0*)	*−87.5* (*−79.8*)

[a] Atom coordinating to the carbene center.

than the different reactivities of the substrates. An analysis of the transition states of the latter reactions will be the subject of future work.

We therefore looked at the trends of the activation barriers for H_2 addition to heterocyclic carbenes **1E–6E** (E = N, P). Fig. 15a shows the trend of the theoretically predicted $\Delta E^{\ddagger}$ values for the calculated reactions. As noted above, PHCs **1P–6P** always have lower activation barriers than NHCs **1N–6N**. The differences are rather small for the pairs of heterocarbenes **5N**/**5P** and **6N**/**6P**. Fig. 15b shows the energy levels of the LUMO of **1E–6E**. There is a clear correlation between the energy differences for LUMO pairs **5N**/**5P** and **6N**/**6P** and the differences between the activation energies. On the other hand, there is no such correlation between the energy levels of the HOMO of **1E–6E**. Fig. 15c shows that the HOMO of PHCs **1P–6P** have nearly the same energy as NHCs **1N–6N**.

It has been pointed out by Frey *et al.*[4] that the higher reactivity of (alkyl)(amino)carbenes compared to diaminocarbenes correlates with a lower singlet–triplet (S/T) gap of the former system. Table 2 compares the activation energies of the hydrogenation energies of **1E–6E** with the S/T gap of the heterocyclic carbenes. It becomes obvious that carbenes where $\Delta E^{\ddagger}$ is small and ΔE_R is large exhibit small S/T gaps. Fig. 16a shows the curves between the calculated S/T values and the theoretically predicted activation energies, and reaction energies, which indicate a linear correlation for both sets of data. However, a closer examination reveals that the S/T gap does not always agree with the trend of the $\Delta E^{\ddagger}$ value. The activation barrier for H_2 addition to unsaturated NHC **2N** (25.0 kcal mol^{-1}) is slightly higher than for saturated NHC **1N** (23.6 kcal mol^{-1}), although the former compound has a smaller S/T gap (58.9 kcal mol^{-1}) than the latter (64.0 kcal mol^{-1}). The same situation is found for the calculated values of $\Delta E^{\ddagger}$ and the S/T gap of **4P** and **5P** (Table 2). Fig. 16b shows the correlation between the activation energies (top) and reaction energies (bottom), and the HOMO–LUMO gap of **1E–6E**.

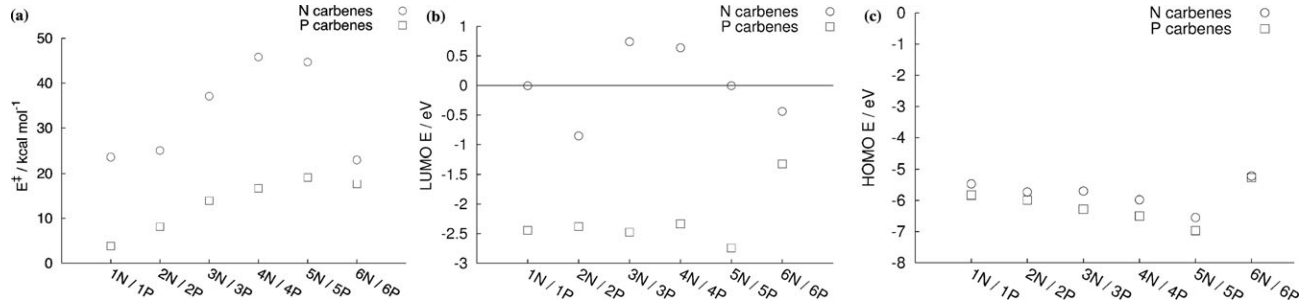

Fig. 15 (a) A plot of the calculated activation barriers, $\Delta E^{\ddagger}$, at CCSD(T)/cc-pVTZ//B3LYP/def-TZVP for the H_2 addition to NHCs **1N–6N** and PHCs **1P–6P**. (b) Plot of the eigenvalues of the LUMO of NHCs **1N–6N** and PHCs **1P–6P** at B3LYP/def-TZVP. (c) Plot of the eigenvalues of the HOMO of NHCs **1N–6N** and PHCs **1P–6P** at B3LYP/def-TZVP.

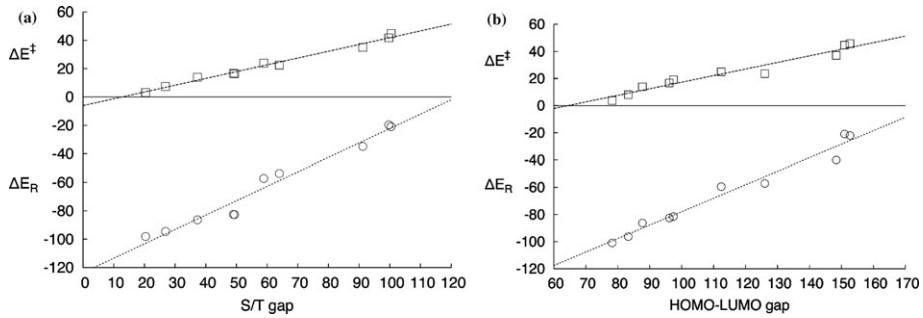

Fig. 16 (a) Correlation of the S/T gap of the PHCs and NHCs at B3LYP/def-TZVP with calculated activation energies $\Delta E^{\ddagger}$ (top) and reaction energies ΔE_R (bottom) at CCSD(T)/cc-pVTZ//B3LYP/def-TZVP. (b) Correlation of the HOMO–LUMO gap of the PHCs and NHCs at B3LYP/def-TZVP with calculated activation energies $\Delta E^{\ddagger}$ (top) and reaction energies ΔE_R (bottom) at CCSD(T)/cc-pVTZ//B3LYP/def-TZVP. Energy values and gaps in kcal mol^{-1}.

Table 2 Calculated activation energies, $\Delta E^{\ddagger}$, and reaction energies, ΔE_R, at the CCSD(T)/cc-pVTZ//B3LYP/def-TZVP level for the reaction of model PHCs **1P–5P** and model NHCs **1N–5N**, and real systems **6N** and **6P**, with H_2. Energy values are given in kcal mol^{-1} and distances in Å

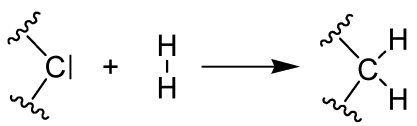

A

A	$\Delta E^{\ddagger}$[a]	ΔE_R[a]	r_{H-H}[b]	S/T gap[c]	HOMO–LUMO gap[d]	$\Sigma\alpha$(E)[e]
1P	3.8 (3.1)	−100.9 (−98.1)	0.810	20.4	78.2	316.8
2P	8.1 (7.3)	−96.2 (−94.5)	0.830	26.9	83.3	324.8
3P	15.2 (13.9)	−87.5 (−86.3)	0.843	37.3	87.7	321.3
4P	19.5 (16.7)	−81.6 (−82.5)	0.838	49.0	96.1	333.1
5P	19.1 (16.4)	−81.5 (−82.7)	0.833	49.4	97.4	337.5/327.4
1N	23.6 (22.5)	−57.1 (−53.7)	1.113	64.4	126.0	359.9
2N	25.0 (23.8)	−59.4 (−57.2)	1.091	58.9	112.4	359.9
3N	37.1 (35.0)	−40.1 (−34.9)	1.368	91.2	148.4	358.7
4N	45.8 (41.7)	−22.0 (−19.7)	1.540	99.7	152.7	360.0
5N	48.5 (44.7)	−22.5 (−21.0)	1.449	100.4	151.0	360.0
6P[17]	(17.7)	(−77.0)	0.921	39.5	91.2	351.2
6N[17]	(23.0)	(−50.4)	1.138	59.8	110.3	360.0

[a] B3LYP/def-TZVP values given in parentheses. [b] Calculated distance of the reacting H_2 molecule in the transition state. [c] S/T gaps at B3LYP/def-TZVP. [d] HOMO–LUMO gap of **1E–6E**. [e] Sum of the bonding angles at the α-heteroatom E = N, P.

The information from Fig. 15c and Fig. 16b suggest that the main factor determining the reactivity of NHCs and PHCs is the energy level of the LUMO of **1E–6E**. Note that the numerical data for the HOMO–LUMO gap, which are also shown in Table 2, have the same trend as the S/T gap.

Are the lower activation barriers and smaller S/T gaps of PHCs caused by the intrinsic effect of the phosphorus atom or do they come from structural changes? It is well known that the stability of carbenes strongly depends on the population of the formally vacant p(π) AO at the divalent carbon atom.

NHCs are stable molecules in the condensed phase because of strong N → C π-donation. Phosphorus can be as powerful a π-donor as nitrogen,[18] but the phosphorus centres in parent PHCs are strongly pyramidalized, which weakens P → C π-donation, while the nitrogen centres in NHCs are planar.[19] Bertrand recognized the problem and solved it by using sterically demanding 2,4,6-tri-*tert*-butyl-phenyl substituents at phosphorus for the synthesis of substituted homologues of **5P**. The X-ray structure analyses of the stable PHCs showed that the sum of the angles at the phosphorus atoms was between 348 and 354°, which is close to a planar arrangement (360°).[9]

The theoretical analysis thus gives a clear picture about the electronic and steric effects on the reactivity of NHCs and PHCs. The N(lp) → C(p_π) donation in NHCs stabilizes the planar structure, which exhibits some aromatic character,[19b] while at the same time, the carbene carbon atom becomes electronically saturated and thus becomes less prone to nucleophilic attack. The P(lp) → C(p_π) donation is weaker than the N(lp) → C(p_π) donation, and thus the pyramidal structure of PHCs becomes electronically more stable than the planar form because the phosphorus lone-pair orbitals in the former species have a significant % s character. The carbene carbon atoms in PHCs are electronically unsaturated, which makes them prone to nucleophilic attack. Bulky substituents at phosphorus may enforce a planar structure for PHCs, which saturates the electronic demand of the carbene carbon atoms in PHCs and thus stabilizes them chemically.

Table 2 also gives the calculated sum of the bonding angles, Σα(E), at the α-heteroatom in **1E–6E** (E = N, P). The data show that PHCs **1P–5P** possess significantly pyramidalized phosphorus centres, while the nitrogen centres in **1N–5N** are essentially planar. However, the phosphorus atom in cyclic alkylphosphinocarbene (CAPC) **6P**, which has bulky 2,6-di-isopropyl-phenyl (DIPP) substituents (Scheme 2), deviates only slightly from a planar arrangement (sum of bond angles 351.2°), and yet it clearly has a lower activation barrier for H_2 addition (17.7 kcal mol^{-1} at B3LYP/def-TZVP) than cyclic alkylamino-carbene (CAAC) **6N** (23.0 kcal mol^{-1} at B3LYP/def-TZVP). The free activation energies at room temperature, which include entropic and thermal effects, are $\Delta E^{\ddagger}_{RT}$ = 27.9 kcal mol^{-1} for **6P** and $\Delta E^{\ddagger}_{RT}$ = 33.1 kcal mol^{-1} for **6N**. Since CAAC **6N** readily splits the H–H bond of H_2 and the N–H bond of NH_3,[4] it seems likely that **6P** should be even more effective in the activation of strong single, and possibly multiple, bonds. Thus, the drawback of PHCs that possess pyramidalized α-heterocentres may be used as an advantage in the hand of a skilful experimentalist because the degree of planarization can be adjusted by a bulky substituent. The goal of synthetic efforts is to find PHCs with large substituents that are bulky enough to stabilize compounds for synthetic purposes and yet preserve a low enough S/T gap to make the carbene prone to addition reactions with C–H, N–H, C–C, *etc*. bonds. The theoretical results reported here may serve as a guideline for such work.

Acknowledgements

This research was supported by the Deutsche Forschungsgemeinschaft. R. T. thanks the Alexander von Humboldt Foundation for a Feodor-Lynen fellowship.

Notes and references

1 A. J. Arduengo III, R. L. Harlow and M. Kline, *J. Am. Chem. Soc.*, 1991, **113**, 2801.
2 (*a*) A. Igau, H. Grützmacher, A. Baceiredo and G. Bertrand, *J. Am. Chem. Soc.*, 1988, **110**, 6463; (*b*) A. Igau, A. Baceiredo, G. Trinquier and G. Bertrand, *Angew. Chem., Int. Ed. Engl.*, 1989, **28**, 621.
3 Recent reviews: (*a*) P. de Frémont, N. Marion and S. P. Nolan, *Coord. Chem. Rev.*, 2009, **253**, 862; (*b*) F. E. Hahn and M. C. Jahnke, *Angew. Chem., Int. Ed.*, 2008, **47**, 3122; (*c*) *N-Heterocyclic Carbenes in Transition-Metal Catalysis*, ed. F. Glorius, Topics in Organometallic Chemistry, Springer, Heidelberg, 2006; (*d*) F. E. Hahn, *Angew. Chem., Int. Ed.*, 2006, **45**, 1348; (*e*) W. Kirmse, *Angew. Chem., Int. Ed.*, 2004, **43**, 1767; (*f*) R. W. Alder, M. E. Blake, M. E. Chaker, J. N. Harvey, F. Paolini and J. Schütz, *Angew. Chem., Int. Ed.*, 2004, **43**, 5896; (*g*) Y. Canac, M. Soleilhavoup, S. Conejero and G. Bertrand, *J. Organomet. Chem.*, 2004, **689**, 3857; (*h*) W. A. Herrmann, *Angew. Chem., Int. Ed.*, 2002, **41**, 1290; (*i*) D. Bourissou, O. Guerret, F. P. Gabbaï and G. Bertrand, *Chem. Rev.*, 2000, **100**, 39.
4 G. D. Frey, V. Lavallo, B. Donnadieu, W. W. Schoeller and G. Bertrand, *Science*, 2007, **316**, 439.
5 (*a*) V. Lavallo, J. Mafhouz, Y. Canac, B. Donnadieu, W. W. Schoeller and G. Bertrand, *J. Am. Chem. Soc.*, 2004, **126**, 8670; (*b*) V. Lavallo, Y. Canac, C. Präsang, B. Donnadieu and G. Bertrand, *Angew. Chem., Int. Ed.*, 2005, **44**, 5705.
6 (*a*) R. Tonner and G. Frenking, *Angew. Chem., Int. Ed.*, 2007, **46**, 8695; (*b*) R. Tonner and G. Frenking, *Chem.–Eur. J.*, 2008, **14**, 3260; (*c*) R. Tonner and G. Frenking, *Chem.–Eur. J.*, 2008, **14**, 3273; (*d*) R. Tonner, F. Öxler, B. Neumüller, W. Petz and G. Frenking, *Angew. Chem., Int. Ed.*, 2006, **45**, 8038; (*e*) M. Alcarazo, C. W. Lehmann, A. Anoop, W. Thiel and A. Fürstner, *Nat. Chem.*, 2009, **1**, 295; (*f*) A. Dyker, V. Lavallo, B. Donnadieu and G. Bertrand, *Angew. Chem., Int. Ed.*, 2008, **47**, 3206.
7 (*a*) W. Petz, C. Kutschera, M. Heitbaum, G. Frenking, R. Tonner and B. Neumüller, *Inorg. Chem.*, 2005, **44**, 1263; (*b*) W. Petz, F. Öxler, B. Neumüller, R. Tonner and G. Frenking, *Eur. J. Inorg. Chem.*, 2009, 4507; (*c*) R. Tonner, G. Heydenrych and G. Frenking, *ChemPhysChem*, 2008, **9**, 1474.
8 M. Rullich, *Diploma Thesis*, Philipps-Universität Marburg, 2008.
9 D. Martin, A. Baceiredo, H. Gornitzka, W. W. Schoeller and G. Bertrand, *Angew. Chem., Int. Ed.*, 2005, **44**, 1700.
10 (*a*) H. Jacobsen, *Dalton Trans.*, 2006, 2214; (*b*) G. Occhipinti, H. R. Bjorsvik and V. R. Jensen, *J. Am. Chem. Soc.*, 2006, **128**, 6952; (*c*) W. W. Schoeller, D. Schroeder and A. B. Rozhenko, *J. Organomet. Chem.*, 2005, **690**, 6079; (*d*) J. D. Masuda, D. Martin, C. Lyon-Saunier, A. Baceiredo, H. Gornitzka, B. Donnadieu and G. Bertrand, *Chem.–Asian J.*, 2007, **2**, 178; (*e*) G. D. Frey, M. Song, J.-B. Bourg, B. Donnadieu, M. Soleilhavoup and G. Bertrand, *Chem. Commun.*, 2008, 4711.
11 (*a*) A. D. Becke, *J. Chem. Phys.*, 1993, **98**, 5648; (*b*) C. Lee, W. Yang and R. Parr, *Phys. Rev. B: Condens. Matter*, 1988, **37**, 785; (*c*) A. Schäfer, C. Huber and R. Ahlrichs, *J. Chem. Phys.*, 1994, **100**, 5829.
12 M. J. Frisch, G. W. Trucks, H. B. Schlegel, G. E. Scuseria, M. A. Robb, J. R. Cheeseman, J. A. Montgomery, Jr., T. Vreven, K. N. Kudin, J. C. Burant, J. M. Millam, S. S. Iyengar, J. Tomasi, V. Barone, B. Mennucci, M. Cossi, G. Scalmani, N. Rega, G. A. Petersson, H. Nakatsuji, M. Hada, M. Ehara, K. Toyota, R. Fukuda, J. Hasegawa, M. Ishida, T. Nakajima, Y. Honda, O. Kitao, H. Nakai, M. Klene, X. Li, J. E. Knox, H. P. Hratchian, J. B. Cross, V. Bakken, C. Adamo, J. Jaramillo, R. Gomperts, R. E. Stratmann, O. Yazyev, A. J. Austin, R. Cammi, C. Pomelli, J. Ochterski, P. Y. Ayala, K. Morokuma, G. A. Voth, P. Salvador, J. J. Dannenberg, V. G. Zakrzewski, S. Dapprich, A. D. Daniels, M. C. Strain, O. Farkas, D. K. Malick, A. D. Rabuck, K. Raghavachari, J. B. Foresman, J. V. Ortiz, Q. Cui, A. G. Baboul, S. Clifford, J. Cioslowski, B. B. Stefanov, G. Liu, A. Liashenko, P. Piskorz, I. Komaromi, R. L. Martin, D. J. Fox, T. Keith, M. A. Al-Laham, C. Y. Peng, A. Nanayakkara, M. Challacombe, P. M. W. Gill, B. G. Johnson, W. Chen, M. W. Wong, C. Gonzalez and J. A. Pople, *GAUSSIAN 03 (Revision E.01)*, Gaussian, Inc., Wallingford, CT, 2004.

13 (*a*) J. Čížek, *J. Chem. Phys.*, 1966, **45**, 4256; (*b*) J. A. Pople, K. Raghavachari, H. B. Schlegel and J. S. Binkley, *Int. J. Quantum Chem.*, 1978, **14**, 545; (*c*) R. J. Bartlett and G. D. Purvis, *Int. J. Quantum Chem.*, 1978, **14**, 561; (*d*) A. K. Wilson, D. E. Woon, K. A. Peterson and T. H. Dunning, Jr., *J. Chem. Phys.*, 1999, **110**, 766.
14 H.-J. Werner, P. J. Knowles, R. Lindh, F. R. Manby, M. Schütz, P. Celani, T. Korona, G. Rauhut, R. D. Amos, A. Bernhardsson, A. Berning, D. L. Cooper, M. J. O. Deegan, A. J. Dobbyn, F. Eckert, C. Hampel, G. Hetzer, A. W. Lloyd, S. J. McNicholas, W. Meyer, M. E. Mura, A. Nicklass, P. Palmieri, R. Pitzer, U. Schumann, H. Stoll, A. J. Stone, R. Tarroni and T. Thorsteinsson, *MOLPRO, version 2006.1: A package of* ab initio *programs*, 2006, see http://www.molpro.net.
15 G. S. Hammond, *J. Am. Chem. Soc.*, 1955, **77**, 334.
16 A possible explanation could be that the dominant orbital interactions for the C–H addition of acetylene to **1N** takes place through the HOMO of the carbene and the C–H vacant σ* orbital of acetylene, while the orbital interactions between acetylene and **1P** occur through the LUMO of the carbene and the occupied C–H orbital. The HOMO of **1N** is energetically higher lying than the HOMO of **1P**, while the LUMO of the latter is lower in energy than the former. Both reactions have higher barriers than the addition reaction through the C–C π-bond. Therefore, the explanation for the different activation barriers of the C–H addition reactions has only theoretical interest.
17 CCSD(T) calculations were not feasible for **6N** and **6P** due to the system size.
18 J. Kapp, C. Schade, A. M. El-Nahasa and P. v. R. Schleyer, *Angew. Chem., Int. Ed. Engl.*, 1996, **35**, 2236.
19 (*a*) D. A. Dixon and A. J. Arduengo III, *J. Phys. Chem.*, 1991, **95**, 4180; (*b*) C. Boehme and G. Frenking, *J. Am. Chem. Soc.*, 1996, **118**, 2039; (*c*) A. Fekete and L. Nyulászi, *J. Organomet. Chem.*, 2002, **643–644**, 278; (*d*) W. W. Schoeller and D. Eisner, *Inorg. Chem.*, 2004, **43**, 2585.